


cy.7

DEC 14 1977

DEC 15 1977



# **ANALYTICAL DESCRIPTION OF THE COMPLETE TWO-DIMENSIONAL TURBULENT BOUNDARY-LAYER VELOCITY PROFILE**

**PROPULSION WIND TUNNEL FACILITY  
ARNOLD ENGINEERING DEVELOPMENT CENTER  
AIR FORCE SYSTEMS COMMAND  
ARNOLD AIR FORCE STATION, TENNESSEE 37389**

**September 1977**

**Final Report for Period October 1976 - March 1977**

Approved for public release; distribution unlimited.

**Prepared for**

**DIRECTORATE OF TEST ENGINEERING  
DEPUTY FOR OPERATIONS  
ARNOLD ENGINEERING DEVELOPMENT CENTER  
AIR FORCE SYSTEMS COMMAND  
ARNOLD AIR FORCE STATION, TENNESSEE 37389**

Proc. 1.1 1.1 1.1 1.1  
1.1 1.1 1.1 1.1  
1.1 1.1 1.1 1.1

## NOTICES

When U. S. Government drawings specifications, or other data are used for any purpose other than a definitely related Government procurement operation, the Government thereby incurs no responsibility nor any obligation whatsoever, and the fact that the Government may have formulated, furnished, or in any way supplied the said drawings, specifications, or other data, is not to be regarded by implication or otherwise, or in any manner licensing the holder or any other person or corporation, or conveying any rights or permission to manufacture, use, or sell any patented invention that may in any way be related thereto.

Qualified users may obtain copies of this report from the Defense Documentation Center.

References to named commercial products in this report are not to be considered in any sense as an endorsement of the product by the United States Air Force or the Government.

This report has been reviewed by the Information Office (OI) and is releasable to the National Technical Information Service (NTIS). At NTIS, it will be available to the general public, including foreign nations.

## APPROVAL STATEMENT

This technical report has been reviewed and is approved for publication.

FOR THE COMMANDER



MARION L. LASTER  
Director of Test Engineering  
Deputy for Operations



ALAN L. DEVEREAUX  
Colonel, USAF  
Deputy for Operations

# UNCLASSIFIED

REPORT DOCUMENTATION PAGE		READ INSTRUCTIONS BEFORE COMPLETING FORM
1. REPORT NUMBER <b>AEDC-TR-77-79</b>	2. GOVT ACCESSION NO.	3. RECIPIENT'S CATALOG NUMBER
4. TITLE (and Subtitle) <b>ANALYTICAL DESCRIPTION OF THE COMPLETE TWO-DIMENSIONAL TURBULENT BOUNDARY-LAYER VELOCITY PROFILE</b>		5. TYPE OF REPORT & PERIOD COVERED <b>Final Report-October 1976 - March 1977</b>
		6. PERFORMING ORG. REPORT NUMBER
7. AUTHOR(s)  <b>David L. Whitfield, ARO, Inc.</b>		8. CONTRACT OR GRANT NUMBER(s)
9. PERFORMING ORGANIZATION NAME AND ADDRESS <b>Arnold Engineering Development Center Air Force Systems Command Arnold Air Force Station, Tennessee 37389</b>		10. PROGRAM ELEMENT, PROJECT, TASK AREA & WORK UNIT NUMBERS <b>Program Element 65807F</b>
11. CONTROLLING OFFICE NAME AND ADDRESS <b>Arnold Engineering Development Center (XRFIS) Arnold Air Force Station, Tennessee 37389</b>		12. REPORT DATE <b>September 1977</b>
		13. NUMBER OF PAGES <b>40</b>
14. MONITORING AGENCY NAME & ADDRESS (if different from Controlling Office)		15. SECURITY CLASS. (of this report)  <b>UNCLASSIFIED</b>
		15a. DECLASSIFICATION/DOWNGRADING SCHEDULE <b>N/A</b>
16. DISTRIBUTION STATEMENT (of this Report)  <b>Approved for public release; distribution unlimited.</b>		
17. DISTRIBUTION STATEMENT (of the abstract entered in Block 20, if different from Report)		
18. SUPPLEMENTARY NOTES  <b>Available in DDC</b>		
19. KEY WORDS (Continue on reverse side if necessary and identify by block number)  <div style="display: flex; justify-content: space-between;"> <div> <b>mathematical analysis</b>  <b>turbulent boundary layer</b>  <b>velocity</b>  <b>profile</b> </div> <div> <b>kinetic energy</b>  <b>functions (mathematics)</b>  <b>walls (smooth impermeable)</b> </div> </div>		
20. ABSTRACT (Continue on reverse side if necessary and identify by block number)  <p>A single analytical expression is derived for the entire (<math>0 &lt; y &lt; \infty</math>) velocity distribution in a two-dimensional, turbulent boundary layer on a smooth impermeable wall. The analytical expression is a linear combination of two trigonometric functions, and the expression depends on the local parameters of skin friction, shape factor, and Reynolds number based on momentum thickness. One of the trigonometric functions is an analytical</p>		

# UNCLASSIFIED

# UNCLASSIFIED

## 20. ABSTRACT (Continued)

solution of the continuity, momentum, and turbulent kinetic energy equations in the inner region of the boundary layer and it depends on the inner variable  $y^+$ . The other trigonometric function is an empirically derived function for the outer region and it depends on the outer variable  $y/\theta$ . The analytical result is validated by numerous comparisons with experimental data which include boundary layers near separation, a reattached boundary layer, nonequilibrium boundary layers, and compressible boundary layers.

## PREFACE

The work reported herein was conducted by the Arnold Engineering Development Center (AEDC), Air Force Systems Command (AFSC), under Program Element 65807F. The results were obtained by ARO, Inc., AEDC Division (a Sverdrup Corporation Company), operating contractor for the AEDC, AFSC, Arnold Air Force Station, Tennessee, under ARO Project No. P33A-G4A. The author of this report is David L. Whitfield, ARO, Inc. Elton R. Thompson is the Air Force project manager. The manuscript (ARO Control No. ARO-PWT-TR-77-43) was submitted for publication on June 16, 1977.

The author would like to acknowledge Dr. J. L. Jacocks, ARO, Inc., with whom periodic discussions were held during the course of this work which contributed appreciably to improving the end result.

## CONTENTS

	<u>Page</u>
1.0 INTRODUCTION . . . . .	5
2.0 ANALYTICAL DEVELOPMENT . . . . .	7
3.0 COMPARISONS WITH EXPERIMENTAL DATA . . . . .	13
4.0 SUMMARY OF RESULTS . . . . .	18
REFERENCES . . . . .	19

## ILLUSTRATIONS

Figure

1. Velocity Distributions According to the Inner Solution (Eq. (2)) and the Experimental Data of Lindgren (Ref. 11) . . . . .	23
2. Reynolds Stress Distributions According to Eq. (3) and the Experimental Data Reported by Schubauer (Ref. 12) . . . . .	24
3. Turbulence Production and Dissipation Distributions According to Eqs. (4) and (5) and the Experimental Data Reported by Schubauer (Ref. 12) . . . . .	25
4. Distributions of the Function $g(y/\theta)$ According to Eqs. (6) and (7) . . . . .	26
5. Correlation of Experimental Velocity Data . . . . .	27
6. Zero, Mild, and Strong Adverse Pressure Gradient Boundary Layers According to Eq. (8) and the Experimental Data of Klebanoff (Ref. 14) and Ludwig and Tillmann (Ref. 6) . . . . .	29
7. Adverse and Favorable Pressure Gradient Boundary Layers According to Eq. (8) and the Experimental Data of Stratford (Ref. 6), Perry (Ref. 6), and Bauer (Ref. 6) . . . . .	30

<u>Figure</u>	<u>Page</u>
8. Comparisons of the Experimental Data of Tillmann (Ref. 6) with Eq. (8) for Boundary Layers Upstream and Downstream of Separation . . . . .	31
9. Airfoil Boundary-Layer Flow Proceeding toward Separation in $u/u_e - y/\theta$ Coordinates . . . . .	32
10. Airfoil Boundary-Layer Flow Proceeding toward Separation in $u^+ - y^+$ Coordinates . . . . .	33
11. Low Reynolds Number, Nonequilibrium, Adverse Pressure Gradient Turbulent Boundary Layers According to Eq. (8) and the Experimental Data of Parikh, Kays, and Moffat (Ref. 16). . . . .	34
12. Experimental Compressible Turbulent Boundary-Layer Data in Transformed Coordinates Compared to Eq. (8) . . .	35
13. Acoustic Research Tunnel (ART) Wall Boundary-Layer Measurements at Mach Numbers of 0.20 and 0.65 Compared to Eq. (8) . . . . .	36
14. LV Data from the Aerodynamic Wind Tunnel (1T) (Tunnel 1T) Bump Experiments (Ref. 22) Compared to Eq. (8) . . . . .	37

### TABLE

1. Summary of Procedure for Computation of Turbulent Boundary-Layer Velocity Distributions . . . . .	38
NOMENCLATURE . . . . .	39

## 1.0 INTRODUCTION

This report is concerned with the development of an analytical expression for the velocity distribution in a turbulent boundary layer. Because numerous velocity distribution expressions have been developed for various portions of a turbulent boundary layer (see, e.g., Ref. 1), a summary of the more recently developed or frequently used methods follows in order to place the present investigation in proper perspective.

A commonly used expression for the turbulent boundary-layer velocity distribution is the logarithmic distribution or law-of-the-wall. The logarithmic velocity distribution is valid in a region near the wall but not in the immediate vicinity of the wall in the so-called viscous sublayer and buffer layer, nor is it valid in the outer part of the boundary layer in the so-called wake region. Particular expressions for the sublayer and buffer layer have been developed (Ref. 1), and a single expression for the sublayer, buffer layer, and logarithmic region was developed by Spalding (Ref. 2). For the outer portion of a turbulent boundary layer, Coles (Ref. 3) developed the law-of-the-wake. Since the appearance of Coles' work, other expressions for the law-of-the-wake were developed which correct certain deficiencies of Coles' (Ref. 3) law-of-the-wake as pointed out by Dean (Ref. 4). Both Spalding's expression (Ref. 2) and the law-of-the-wake were developed such that they asymptote to the logarithmic velocity distribution. Dean (Ref. 4) used this feature of commonality in asymptotic behavior to combine Spalding's (Ref. 2) expression and a law-of-the-wake to obtain one unified expression that is valid from the wall to the outer edge of the boundary layer. Dean's expression, however, cannot be written such that either the velocity,  $u$ , or the distance from the wall,  $y$ , is an explicit function of the other. This is a consequence of using Spalding's (Ref. 2) expression which gives  $y^+$  explicitly in terms of  $u^+$ . The law-of-the-wake used by Dean (Ref. 4) contains Coles' profile parameter,  $\Pi$ . In general,  $\Pi$  is determined by locating or choosing  $\delta$  (which Clauser (Ref. 5)



calls an ill-defined quantity) and then using the law-of-the-wake to solve for  $\Pi$ ; or,  $\Pi$  and  $\delta$  are solved for simultaneously using the law-of-the-wake. For example, in the matching of Coles' law-of-the-wake as given in Ref. 6, with the data presented in the Stanford Conference Proceedings (Ref. 6), both  $\Pi$  and  $\delta$  were used as free parameters. The values of  $\delta$  given in Ref. 6 varied considerably from values corresponding to the usual definition of  $\delta$ , where, for example,  $\delta$  is the value of  $y$  where  $u/u_e = 0.99$ . Therefore, based on this brief summary of available analytical techniques, a contribution in this area would be to analytically describe turbulent boundary-layer velocity distributions by an expression that gives the velocity explicitly as a function of distance from the wall, and that contains parameters which are explicitly defined and can be calculated in terms of properties of the boundary layer. The purpose of this report is to develop such an expression and validate it by comparisons with experimental data. The resulting expression should be useful for making hand calculations of complete turbulent boundary-layer velocity profiles, providing initial conditions for numerical solutions of the boundary-layer equations, and for use in integral boundary-layer theories.

Attention here is focused on two-dimensional turbulent boundary layers on smooth impermeable walls. The approach taken is the construction of a composite expression in terms of the inner variable  $y^+$  and the outer variable  $y/\theta$ . An analytical solution of the turbulent boundary-layer equations (including a turbulent kinetic energy equation) for the region near the wall (Ref. 7) is used for the inner solution, and an empirical expression is derived for the outer region of the boundary layer. The analytical development is given in the following section and the accuracy of the analytical result is investigated in Section 3.0 by comparisons with a variety of experimental data, which include boundary layers near separation, a boundary layer downstream of reattachment, nonequilibrium boundary layers, and compressible boundary layers. A summary of the procedure and equations for the computation of turbulent boundary-layer velocity distributions is given in Table 1.

## 2.0 ANALYTICAL DEVELOPMENT

The derivation of the analytical result is contained in this section. The development is carried out with all variables in incompressible form. In the following section, comparisons are made with compressible data and at that point the variables will be transformed to account for compressibility.

The desired composite expression is required to have the following properties: (1) recover the solution developed in Ref. 7 for the inner region, i.e.,  $y^+ < 0(10^2)$ , (2) approach the proper limiting value of  $u^+ \rightarrow u_e^+$  (or  $u/u_e \rightarrow 1$ ) as  $y \rightarrow \infty$ , and (3) recover the velocity profiles similar to those correlated by von Doenhoff and Tetervin (Ref. 8) away from the wall in the outer variable  $y/\theta$ . Requirement number (1) comprises the inner solution denoted as  $u_1^+$  and requirements (2) and (3) comprise the outer solution denoted as  $u_o^+$ . The composite solution  $u^+$  is taken as

$$u^+ = u_1^+ + u_o^+ \quad (1)$$

Consideration is now given to particular expressions for  $u_1^+$  and  $u_o^+$ .

The derivation of the inner solution is given in detail in Ref. 7. It was obtained from an analytical solution of the turbulent boundary-layer equations including a turbulent kinetic energy equation which was developed in Ref. 7 for turbulence modeling. The primary assumptions made in obtaining the inner solution were:

1. the total shear stress consisted of the molecular and turbulent contributions, was constant, and equal to the wall value,  $\tau_w$ ,
2. the density was constant and equal to the wall value,  $\rho_w$ ,

3. the turbulent kinetic energy was proportional to  $-\overline{u'v'}$ , and
4. the turbulent kinetic energy, or  $-\overline{u'v'}$ , was an explicit function of  $u^+$ .

Assumption (1) is commonly used in the region near the wall and assumption (2) was used to satisfy  $\tau_w = (\mu \partial u / \partial y)_y \rightarrow 0$  because  $u^+ = y^+$  when  $y \rightarrow 0$ . Assumption (3) is not an uncommon assumption in the fully turbulent part of a boundary layer (see, e.g., Ref. 7 for some history of the use and development of this relation); however, some supporting evidence is desirable to justify this approximation for use in the inner region. Such evidence is given, for example, by Fig. 5 of Hanjalić and Launder (Ref. 9) where they compared their numerical calculations of turbulent kinetic energy and shear stress ( $-\overline{u'v'}$ ) with experimental data in the inner region ( $y^+ < 0(10^2)$ ). If one traces their calculations of  $-\overline{u'v'}/u_\tau^2$  as a function of  $y^+$  and overlays it on their calculations of turbulent kinetic energy, one finds that the distributions are similar except for  $y^+$  less than about 3. For  $y^+ < 3$ , their calculations of  $-\overline{u'v'}/u_\tau^2$  fall below the experimental data. In considering some of the data presented by Hanjalić and Launder in Fig. 5 of Ref. 9, Hinze (Ref. 10) observed that, whereas it can be proved that  $-\overline{u'v'}$  must behave as  $y^{+3}$  or  $y^{+4}$  as  $y^+ \rightarrow 0$ , experimental data indicate that  $-\overline{u'v'} \sim y^{+2}$  for  $y^+$  as small as measurements are currently available which is about  $y^+$  of  $0(10^0)$ . This experimentally observed quadratic variation of  $-\overline{u'v'}/u_\tau^2$  with  $y^+$  near the wall is consistent with the experimentally observed and numerically calculated distributions of turbulent kinetic energy near the wall (see, e.g., Ref. 9, Fig. 5 again). Therefore, based on these experimental and numerical distributions of turbulent kinetic energy and shear stress, assumption (3) appears reasonable in the inner region as well as the outer portion of the boundary layer although the constants of proportionality may differ. Assumption (4) is a consequence of the fact that both  $u^+$  and  $-\overline{u'v'}$  are functions of  $y^+$  in the inner region, and hence  $-\overline{u'v'}$  is a function of  $u^+$ .

The solution procedure in Ref. 7 was to solve the turbulent kinetic energy equation for  $-\overline{u'v'}$  as a function of  $u^+$  (recall that the turbulent kinetic energy was assumed proportional to  $-\overline{u'v'}$ ). Then  $-\overline{u'v'}$  was used in the expression for the total shear stress (which was assumed constant and equal to the wall value) to obtain a first-order differential equation for the velocity. This first-order equation was obtained by normalizing the expression for the total shear stress,  $\tau_w = \mu(\partial u/\partial y) - \rho \overline{u'v'}$ , which resulted in the equation  $du_1^+/dy^+ - \rho \overline{u'v'}/u_1^{+2} = 1$ . This equation was then solved with the boundary condition  $u_1^+ = 0$  at  $y^+ = 0$  to obtain the solution for  $u_1^+$  as a function of  $y^+$  (see Ref. 7).

The significance of the results of Ref. 7 is that a consistent description of mean turbulence quantities in the inner region was obtained in exceedingly simple mathematical form. This is indicated by Figs. 1, 2, and 3 and the corresponding inner solutions for the velocity, Reynolds stress, turbulence production, and direct dissipation of mean-flow energy given, respectively, as

$$u_1^+ = \frac{1}{0.09} \tan^{-1} (0.09y^+) \quad (2)$$

$$\frac{-\overline{u'v'}}{u_1^+} = \frac{(0.09y^+)^2}{1 + (0.09y^+)^2} \quad (3)$$

$$\frac{-\overline{u'v'}}{u_1^+} \frac{du_1^+}{dy^+} = \left( \frac{0.09y^+}{1 + (0.09y^+)^2} \right)^2 \quad (4)$$

$$\left( \frac{du_1^+}{dy^+} \right)^2 = \left( \frac{1}{1 + (0.09y^+)^2} \right)^2 \quad (5)$$

Note from Eq. (2) that the classical sublayer result of  $u_1^+ = y^+$  is recovered for small values of  $y^+$ . Also of interest is the accuracy in the slope of the velocity distribution as indicated by the comparison of the dissipation term [Eq. (5)] with experimental data in Fig. 3. The Reynolds stress and turbulence production comparisons are included to complete the turbulence modeling description according to the inner solution and illustrate its simplicity and good agreement with experimental data.

In contrast to  $u_1^+$ ,  $u_o^+$  does not have a theoretical background. It is derived here in the same spirit as Coles' (Ref. 3) law-of-the-wake. The outer variable, however, is taken as  $y/\theta$  rather than  $y/\delta$  and the end result is entirely different from the law-of-the-wake. Note from Eq. (2) that as  $y^+ \rightarrow \infty$ ,  $u_1^+ \rightarrow \pi/0.18$ . Therefore, according to Eq. (1), for  $u^+$  to have the proper limiting value of  $(2/c_f)^{1/2}$  as  $y \rightarrow \infty$ ,  $u_o^+$  must behave as

$$u_o^+ \rightarrow \left[ \left( \frac{2}{c_f} \right)^{1/2} - \frac{\pi}{0.18} \right]$$

as  $y \rightarrow \infty$ . Furthermore, because  $u_1^+$  gives the desired result for small  $y$ ,  $u_o^+$  must behave as  $u_o^+ \rightarrow 0$  as  $y \rightarrow 0$ . Therefore, the form

$$u^+ = \frac{1}{0.09} \tan^{-1} (0.09y^+) + \left[ \left( \frac{2}{c_f} \right)^{1/2} - \frac{\pi}{0.18} \right] g\left(\frac{y}{\theta}\right) \quad (6)$$

is considered. Actually  $g(y/\theta)$  will depend on  $c_f$ ,  $H$ , and  $Re_\theta$ , but regardless of the values of these parameters, the function  $g(y/\theta)$  must behave as  $g(0) = 0$  and  $g(\infty) \rightarrow 1$ .

The criterion for choosing the function  $g(y/\theta)$  was that it be a relatively simple function that does a reasonable job of describing the trend of experimental velocity data. The experimental data trends were investigated by solving for  $g(y/\theta)$  from Eq. (6), using experimental data for  $u^+$ ,  $y^+$ , and  $c_f$ , and plotting  $g(y/\theta)$  versus  $y/\theta$ . An example of the trends is given in Fig. 4 for favorable and highly adverse pressure

gradient flows. (These data, as are many of the data used in this report, were taken from the tabulations given in the Stanford Conference Proceedings (Ref. 6).) The analytical function used here to describe the distribution of the data is

$$g\left(\frac{y}{\theta}\right) = \tanh^{1/2} \left[ a \left( \frac{y}{\theta} \right)^b \right] \quad (7)$$

where  $a$  and  $b$  are parameters that are constant for a given boundary-layer profile and are functions of  $c_f$ ,  $H$ , and  $Re_\theta$ . The complete velocity distribution is therefore given by

$$u^+ = \frac{1}{0.09} \tan^{-1} (0.09 y^+) + \left[ \left( \frac{2}{c_f} \right)^{1/2} - \frac{\pi}{0.18} \right] \tanh^{1/2} \left[ a \left( \frac{y}{\theta} \right)^b \right] \quad (8)$$

where

$$\left( \frac{2}{c_f} \right)^{1/2} = \frac{u_c^+}{u_e^+}, \quad y^+ = \frac{Re_\theta y}{u_e^+ \theta}, \quad \text{and} \quad \frac{u}{u_e} = \frac{u^+}{u_e^+}$$

The parameters  $a$  and  $b$  are determined by satisfying requirement number (3), which is that velocity profiles similar to those correlated by von Doenhoff and Tetervin (Ref. 8) be recovered away from the wall in the outer variable  $y/\theta$ . The precise profiles established in Ref. 8 are not recovered because of the fact that presumably more accurate data were obtained subsequent to the publication date of Ref. 8 (1943), and also because a Reynolds number effect on the velocity profiles was reported (see, e.g., Ref. 13) subsequent to the appearance of Ref. 8. Nevertheless, the idea of von Doenhoff and Tetervin is what is important in this work, and that is that turbulent boundary-layer velocity distributions can be correlated (at least approximately in view of the Reynolds number effect) in a one-parameter family of curves of  $u/u_e$  versus  $y/\theta$ , with each curve corresponding to a constant shape factor  $H$ . Specifically,  $a$  and  $b$  are determined by matching the distribution  $u/u_e$  at two points,  $y/\theta = 2$  and  $y/\theta = 5$ . The point  $y/\theta = 2$  was selected because it lies relatively close to the wall and yet is outside the

region where the inner solution is valid (except for extremely low Reynolds number flows), and  $y/\theta = 5$  was selected because it represents the outer region and is a point in the boundary layer where the velocity ratio,  $u/u_e$ , is relatively constant for all  $H$  as demonstrated in Ref. 8.

The variation of  $u/u_e(2)$  ( $u/u_e$  at  $y/\theta = 2$ ) with  $H$  is illustrated in Fig. 5a by the experimental data tabulated in Ref. 6. An expression which represents these data reasonably well is  $u/u_e = 1.723 \exp(-0.6H)$  as shown in Fig. 5a. The experimental data of Ref. 6 are for the most part high Reynolds number data, and data for  $Re_\theta > 10^4$  were used in Fig. 5a. The effect of Reynolds number is to increase the ratio  $u/u_e(2)$  as  $Re_\theta$  decreases below about  $10^4$ . Charts were established by Thompson (Ref. 13) which illustrated this trend, and these were used as a guide in estimating the effect of  $Re_\theta$  on  $u/u_e(2)$ . An empirical expression which accounts for the variation of  $u/u_e(2)$  with  $H$  and  $Re_\theta$  is given by

$$\frac{u}{u_e}(2) = 1.723e^{-0.6H} \left( 1 + \frac{50}{Re_\theta} \right) \quad (9)$$

The variation of  $u/u_e(5)$  ( $u/u_e$  at  $y/\theta = 5$ ) with  $H$  is illustrated in Fig. 5b, again using the experimental data of Ref. 6. Thompson's charts (Ref. 13) indicate a Reynolds number effect for these  $u/u_e(5)$  data also. However, the trend suggested by the charts in Ref. 13 does not appear to be entirely substantiated by the experimental data of Ref. 6. Therefore, the Reynolds number effect is neglected for these velocity ratio correlations at  $y/\theta = 5$ , and the expression used to correlate the data in Fig. 5b (which includes data for  $Re_\theta > 3,000$ ) is given by

$$\frac{u}{u_e}(5) = 0.87 + 0.08e^{-2.6(H-1.95)^2} \quad (10)$$

Note in Fig. 5a the data extend to larger  $H$  than in Fig. 5b. The data in Fig. 5a for  $H > 2.9$  are measurements made by Fraser (Ref. 6) in a round diffuser. The significance of this is that these axisymmetric internal flow measurements correlate well with the two-dimensional data

for  $y/\theta = 2$ , but these data do not correlate with the two-dimensional data for  $y/\theta = 5$ . Therefore, for axisymmetric flows, the correlation given by Eq. (10) should be modified.

Using Eqs. (9) and (10), the parameters  $a$  and  $b$  can be calculated as described in detail in Table 1. Table 1 is simply a summary of the solution of Eq. (8) for  $a$  and  $b$  at the two points  $y/\theta = 2$  and 5. The curves given in Fig. 4 were obtained using Eq. (7) with  $a$  and  $b$  calculated in this manner. The distributions given by Eq. (7) in Fig. 4 are fair representations of the experimental data, particularly in view of the fact that any discrepancies in Fig. 4 are amplified because the experimental data were referenced to  $u_i^+$  and normalized by  $\left[\left(\frac{2}{c_f}\right)^{1/2} - \frac{\pi}{0.18}\right]$ , i.e., the ordinate in Fig. 4 is given by using the experimental data to evaluate

$$(u^+ - u_i^+) / \left[ \left( \frac{2}{c_f} \right)^{1/2} - \frac{\pi}{0.18} \right]$$

Comparisons of Eq. (8) with experimental data in conventional plots of  $u^+$  versus  $y^+$  and  $u/u_e$  versus  $y/\theta$  are given in the following section.

### 3.0 COMPARISONS WITH EXPERIMENTAL DATA

The experimental data selected for comparisons with Eq. (8) are intended to represent examples weighted to flows that are considered difficult to calculate or correlate, as opposed to flows that are readily calculated or correlated. For example, emphasis is given to comparisons with boundary layers near separation, reattached boundary layers, and nonequilibrium boundary layers. In addition, compressible turbulent boundary-layer data are compared with Eq. (8).

The much used experimental data of Klebanoff (Ref. 14) and Ludwig and Tillmann (Ref. 6) are compared with Eq. (8) in Fig. 6 in the variables  $u^+$  and  $y^+$ . In Fig. 6 the comparisons involve zero and mild adverse pressure gradient flows as indicated by the values of  $\beta$  (where



$\beta = \frac{\delta^*}{\tau_w} \frac{dp}{dx}$  ) of 0.0 and 5.499. Also, a comparison is made with a profile ( $\beta = 2.996$ ) which comes from the group of data Ludwig and Tillmann labeled strong adverse pressure gradient. Actually, this  $\beta = 2.996$  profile was measured just downstream of the location of the strongest pressure gradient, and the rate of change of pressure gradient was large. In all three examples given in Fig. 6, the agreement between Eq. (8) and the experimental data is considered good.

In Fig. 7 comparisons in  $u^+ - y^+$  coordinates are made between Eq. (8) and two adverse pressure gradient flows and one favorable pressure gradient flow. The data of Perry (Ref. 6) were taken in a decreasing adverse pressure gradient flow and resemble (Ref. 6) the flow in a straight-walled diffuser. Stratford's data (Ref. 6) were taken downstream of an abrupt onset of severe positive pressure gradient. Both Perry and Stratford's data are out of equilibrium (equilibrium requires  $\beta$  to be invariant in the streamwise direction) and Stratford's data are near separation. Bauer's measurements (Ref. 6) were made in water falling down a plate-glass surface, and this boundary layer was near equilibrium. The agreement between Eq. (8) and the data in Fig. 7 is considered good. Note that there is little, if any, logarithmic region remaining in Stratford's profile.

A difficult test for Eq. (8) was thought to be that provided by the experiments of Tillmann (Ref. 6) concerning reattachment and recovery from separation at a ledge spoiler. These experiments were stated in Ref. 6 to be among the best available concerning this problem. Comparisons are made in Fig. 8 between Eq. (8) and four of Tillman's profiles in  $u/u_e - y/\theta$  coordinates. The two profiles nearest the ledge, as indicated by the circle and square symbols in the insert in Fig. 8, are also the nearest ones to the ledge which were reported in Ref. 6. The agreement in Fig. 8 is considered reasonably good.

Of practical interest for aerodynamic testing are the measurements by Newman (Ref. 6) of an airfoil boundary layer proceeding toward separation. Two profiles of Newman (Ref. 6) are compared with Eq. (8) in Fig. 9 in  $u/u_e - y/\theta$  coordinates. The profile of the last axial station reported in Ref. 6 is used in Fig. 9 ( $\beta = 182.776$ ) because it was near separation, and the other profile was chosen arbitrarily and has a  $\beta$  of about one order of magnitude less ( $\beta = 14.541$ ). The agreement between Eq. (8) and the experimental profile for  $\beta = 182.776$  is not as good as the agreement between Eq. (8) and the experimental profile for  $\beta = 14.541$ . The former, however, is considered acceptable and the latter extremely good. Winter (Ref. 15) observed that a logarithmic region does not exist for the highly adverse pressure gradient profile ( $\beta = 182.776$ ) shown in Fig. 9. From Fig. 10, where these same data are presented in  $u^+ - y^+$  coordinates, one can easily see Winter's point. The analytical logarithmic relation, given in Fig. 10 for reference, contains the constants suggested by Coles (Ref. 6). Acceptable agreement is, therefore, obtained between Eq. (8) and an experimental turbulent boundary-layer profile that has no logarithmic region.

Some recent measurements by Parikh, Kays, and Moffat (Ref. 16) in low Reynolds number, nonequilibrium, adverse pressure gradient boundary layers are compared with Eq. (8) in Fig. 11. The profile with  $H = 2.002$  was chosen for comparison because it had both the largest value of  $H$  and  $\beta$  of all the profiles reported in Ref. 16. The remaining profile in Fig. 11 was chosen to represent an extremely low Reynolds number test. The agreement in Fig. 11 between Eq. (8) and the experimental data is considered reasonably good. However, depending on  $c_f$  and  $H$ , the data in Fig. 11 for  $Re_\theta = 1,220$  are near the conditions where the point  $y/\theta = 2$  may not be outside the region where the inner solution is valid. In this case a different point, located outside  $y/\theta = 2$ , should be used in place of the point at  $y/\theta = 2$  for determining parameters  $a$  and  $b$ .

Compressible turbulent flows are now investigated from the point of view of applying Eq. (8) directly, using equivalent incompressible values for the variables in Eq. (8), and assessing the quality of agreement with experimental data. To this end, the transformation theory of Lewis, Kubota, and Webb (Ref. 17) is considered. Lewis, Kubota, and Webb suggested the coordinates

$$\frac{u}{u_e} = \frac{\bar{u}}{\bar{u}_e} \quad (11)$$

and

$$\frac{\bar{y}}{\bar{\theta}} = \int_0^y \frac{\rho}{\rho_e} \frac{dy}{\bar{\theta}_e} \quad (12)$$

The superscript bar ( $\bar{\phantom{x}}$ ) notation was used in Ref. 17 and refers to low-speed flow. Therefore,  $\bar{y}/\bar{\theta}$  is taken as the outer variable  $y/\theta$  in Eq. (8). The variables defined by Eqs. (11) and (12) were used in Fig. 2 of Ref. 17 to correlate a large amount of high Mach number constant pressure turbulent boundary-layer data. Figure 2 of Ref. 17 is used as Fig. 12 of this report, with an additional curve representing Eq. (8). Equivalent incompressible variables for Eq. (8), which correspond to the compressible data in Fig. 12, were determined as follows. The "law of corresponding stations" (Ref. 20) is the relation

$$c_f Re_\theta = \frac{\rho_e \mu_e}{\rho_w \mu_w} (c_f)_c (Re_\theta)_c \quad (13)$$

Assuming a constant pressure normal to the surface and a linear variation of viscosity with temperature as was used in Ref. 17, Eq. (13) reduces to

$$c_f Re_\theta = (c_f)_c (Re_\theta)_c \quad (14)$$

All the data in Fig. 12 are for  $5 < (c_f)_c (Re_\theta)_c < 9$ . Using Eq. (14) and a mean value of  $(c_f)_c (Re_\theta)_c = 7$ , one has that  $c_f Re_\theta = 7$ . Using the skin friction correlation of Winter and Gaudet (Ref. 21) for constant pressure turbulent boundary layers, and the mean value of  $c_f Re_\theta = 7$ ,

one has that  $c_f = 0.0035$  and  $Re_\theta = 2,000$ , approximately. A representative, incompressible shape factor for the constant pressure turbulent boundary-layer data in Fig. 12 is taken as 1.3 based on those tabulated in Ref. 21 for compressible flows at higher Reynolds numbers. Therefore, Eq. (8) was evaluated for the equivalent incompressible values of  $c_f = 0.0035$ ,  $Re_\theta = 2,000$ , and  $H = 1.3$ . The agreement in Fig. 12 is considered good, particularly so, in view of the fact that hypersonic data up to Mach number 8.18 are included. Scatter in the experimental data in Fig. 12 for small  $\bar{y}/\bar{\theta}$  is attributed in Ref. 17 to the lack of accounting for viscous dissipation effects in the transformation theory. The curves marked equivalent incompressible profiles in Fig. 12 were placed there by Lewis, Kubota, and Webb (Ref. 17) (recall that Fig. 12 was taken from Ref. 17). Obviously, Eq. (8) provides a marked improvement of correlating these data over that provided by the equivalent incompressible profiles included in Fig. 12.

Recent solid tunnel wall measurements were made\* in the Propulsion Wind Tunnel Facility (PWT) Acoustic Research Tunnel (ART) at the Arnold Engineering Development Center (AEDC). Two of the measured profiles representing the low and high Mach numbers investigated,  $M_e = 0.20$  and 0.65, are compared with Eq. (8) in Fig. 13. Although the larger Mach number is only 0.65, it is sufficiently large that compressibility should be taken into account, particularly with regard to the shape factor  $H$ . Compressibility was taken into account by first reducing these measurements (which were pitot pressure measurements) by the data reduction method described in Ref. 7 for the appropriate free-stream conditions. The resulting velocity profiles were then used to obtain the corresponding incompressible values of  $H$ ,  $Re_\theta$ , and  $c_f$  for use in Eq. (8). Relatively good agreement between Eq. (8) and the experimental data is demonstrated in Fig. 13.

---

\*These measurements were made by Dr. J. A. Benek, ARO, Inc.

Boundary-layer measurements have recently been reported by Altstatt (Ref. 22) of transonic flow over a one-inch-high, twelve-inch-long circular arc bump placed in the floor (a solid floor was used) of the PWT Aerodynamic Wind Tunnel (1T) at AEDC. A schematic of the flow and identification of the location of the measurements are given in the insert in Fig. 14. The data indicated by the square symbols were taken in the cusp region where the wall is faired into the bump. These particular measurements were made by Cline (Ref. 22) using a Laser Doppler Velocimeter (LV) system. Compressibility was accounted for by the method described above for the ART data, except that velocity data were available directly from the measurements because an LV system was used. The agreement between Eq. (8) and the experimental data in Fig. 14 is reasonably good, particularly with regard to the measurements in the cusp region.

#### 4.0 SUMMARY OF RESULTS

An analytical expression for the velocity distribution in a turbulent boundary layer was derived and shown to be in good agreement with the experimental data considered over the entire domain  $0 \leq y < \infty$ . The analytical expression recovers experimental velocity distributions in the region near the wall, matches correlated velocity distributions at  $y/\theta = 2$  and 5, and gives the proper limiting velocity as  $y \rightarrow \infty$ . The resulting expression gives velocity explicitly as a function of  $y$  and depends on properties that are explicitly defined.

A distinguishing feature of the inner solution results is that besides the good agreement between the inner solution and velocity distribution data in the region near the wall, good agreement was also obtained with Reynolds stress, turbulence production, and turbulence dissipation data. To the extent of obtaining this agreement with experimental data, the inner solution is therefore consistent in that the same model represents all these mean turbulence quantities simultaneously. An additional feature is that the expressions for these turbulence quantities are exceedingly simple.

The single major difference between the present analytical expression of the turbulent boundary layer velocity distribution and preceding expressions is the absence of an explicit logarithmic term. This absence of a logarithmic term is completely contrary to years of tradition in turbulent boundary-layer research, but was the primary result which eventually led to the development of a single expression that provided a reasonably good description of the entire ( $0 \leq y < \infty$ ) velocity profile. The present result is, no doubt, not the final word concerning velocity distribution expressions. However, the important result of the present investigation might be the demonstration that analytical forms other than a logarithmic distribution (which, incidently, Coles (Ref. 3) contends is empirical because, among other things, of the requirement that the total shear stress must remain constant if the logarithmic term is to be derived analytically, and this requirement contradicts experimental observations in that the logarithmic distribution can be a good representation of the actual velocity distribution in regions where experiments demonstrate that the total shear stress is not constant) should receive further attention.

## REFERENCES

1. Jayatilke, C. L. V. "The Influence of Prandtl Number and Surface Roughness on the Resistance of the Laminar Sub-Layer to Momentum and Heat Transfer." In Progress in Heat and Mass Transfer, Vol. 1, Pergamon Press, New York, 1969, pp. 193-329.
2. Spalding, D. B. "A Single Formula for the "Law of the Wall"." Journal of Applied Mechanics, Transactions of the ASME, Series E., Vol. 28, September 1961, pp. 455-458.
3. Coles, D. "The Law of the Wake in the Turbulent Boundary Layer." Journal of Fluid Mechanics, Vol. 1, 1956, pp. 191-226.

4. Dean, R. B. "A Single Formula for the Complete Velocity Profile in a Turbulent Boundary Layer." Journal of Fluid Engineering, Transactions of the ASME, December 1976, pp. 723-727.
5. Clauser, F. H. "The Turbulent Boundary Layer." In Advances in Applied Mechanics, Vol. 4, New York, 1956, pp. 1-51.
6. Coles, D. E. and Hirst, E. A., Editors. "Proceedings Computation of Turbulent Boundary Layers - 1968 AFOSR-IFP-Stanford Conference." Vol. II Compiled Data, Stanford University, Stanford U.S.A.
7. Whitfield, D. L. "Analytical, Numerical, and Experimental Results on Turbulent Boundary Layers." AEDC-TR-76-62, July 1976.
8. von Doenhoff, A. E. and Tetervin, N. "Determination of General Relations for the Behavior of Turbulent Boundary Layers." NACA Report No. 772, 1943.
9. Hanjalić, K. and Launder, B. E. "Contribution Towards a Reynolds-Stress Closure for Low-Reynolds-Number Turbulence." Journal of Fluid Mechanics, Vol. 74, Part 4, 1976, pp. 593-610.
10. Hinze, J. O. Turbulence. Second Edition, McGraw-Hill, Inc., New York, 1975, Chapter 7.
11. Lindgren, E. R. "Experimental Study on Turbulent Pipe Flows of Distilled Water." Department of Civil Engineering, Oklahoma State University, Report 1, AD621071, 1965.
12. Schubauer, G. B. "Turbulent Processes as Observed in Boundary Layer and Pipe." Journal of Applied Physics, Vol. 25, No. 2, February 1954, pp. 188-196.

13. Thompson, B. G. J. "A New Two-Parameter Family of Mean Velocity Profiles for Incompressible Turbulent Boundary Layers on Smooth Walls." Aeronautical Research Council, London, Reports and Memoranda No. 3463, April 1965.
14. Klebanoff, P. S. "Characteristics of Turbulence in a Boundary Layer with Zero Pressure Gradient." NACA Report 1247, 1955.
15. Winter, K. G. "An Outline of the Techniques Available for the Measurement of Skin Friction in Turbulent Boundary Layers." Compressible Turbulent Boundary Layers, Vol. I, Lecture Series 86, von Karman Institute for Fluid Dynamics, March 1-5, 1976.
16. Parikh, P. G., Kays, W. M., and Moffat, R. J. "A Study of Adverse Pressure Gradient Turbulent Boundary Layers with Outer Region Non-Equilibrium." Report No. HMT-26, Thermosciences Division, Department of Mechanical Engineering, Stanford University, July 1976.
17. Lewis, J. E., Kubota, T., and Webb, W. H. "Transformation Theory for the Adiabatic Compressible Turbulent Boundary Layer with Pressure Gradient." AIAA Journal, Vol. 8, No. 9, September 1970, pp. 1644-1650.
18. Coles, D. "Measurements in the Boundary Layer on a Smooth Flat Plate in Supersonic Flow. III. Measurements in a Flat-Plate Boundary Layer at the Jet Propulsion Laboratory." Report No. 20-71, Jet Propulsion Laboratory, Pasadena, California, June 1, 1953.
19. Lobb, R. K., Winkler, E. M., and Persh, J. "NOL Hypersonic Tunnel No. 4 Results VII: Experimental Investigation of Turbulent Boundary Layers in Hypersonic Flow." NAVORD Report R 3880, 1955, Naval Ordnance Lab, White Oak, Maryland.



20. Coles, D. E. "The Turbulent Boundary Layer in a Compressible Fluid." R-403-PR, September 1962, Rand Corporation, Santa Monica, California.
21. Winter, K. G. and Gaudet, L. "Turbulent Boundary-Layer Studies at High Reynolds Numbers at Mach Numbers Between 0.2 and 2.8." Aeronautical Research Council, London, Reports and Memoranda No. 3712, December 1970.
22. Altstatt, M. C. "An Experimental and Analytic Investigation of a Transonic Shock-Wave/Boundary-Layer Interaction." AEDC-TR-77-47, May 1977.

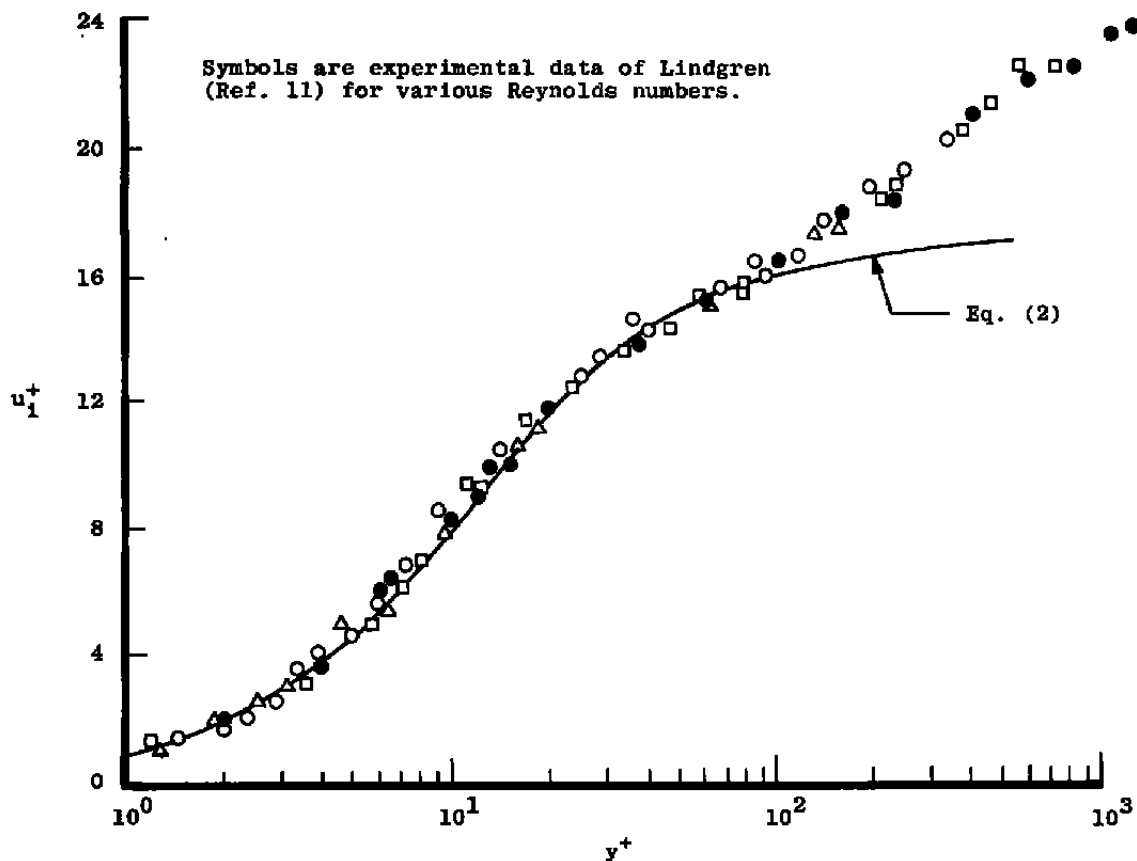


Figure 1. Velocity distributions according to the inner solution (Eq. (2)) and the experimental data of Lindgren (Ref. 11).

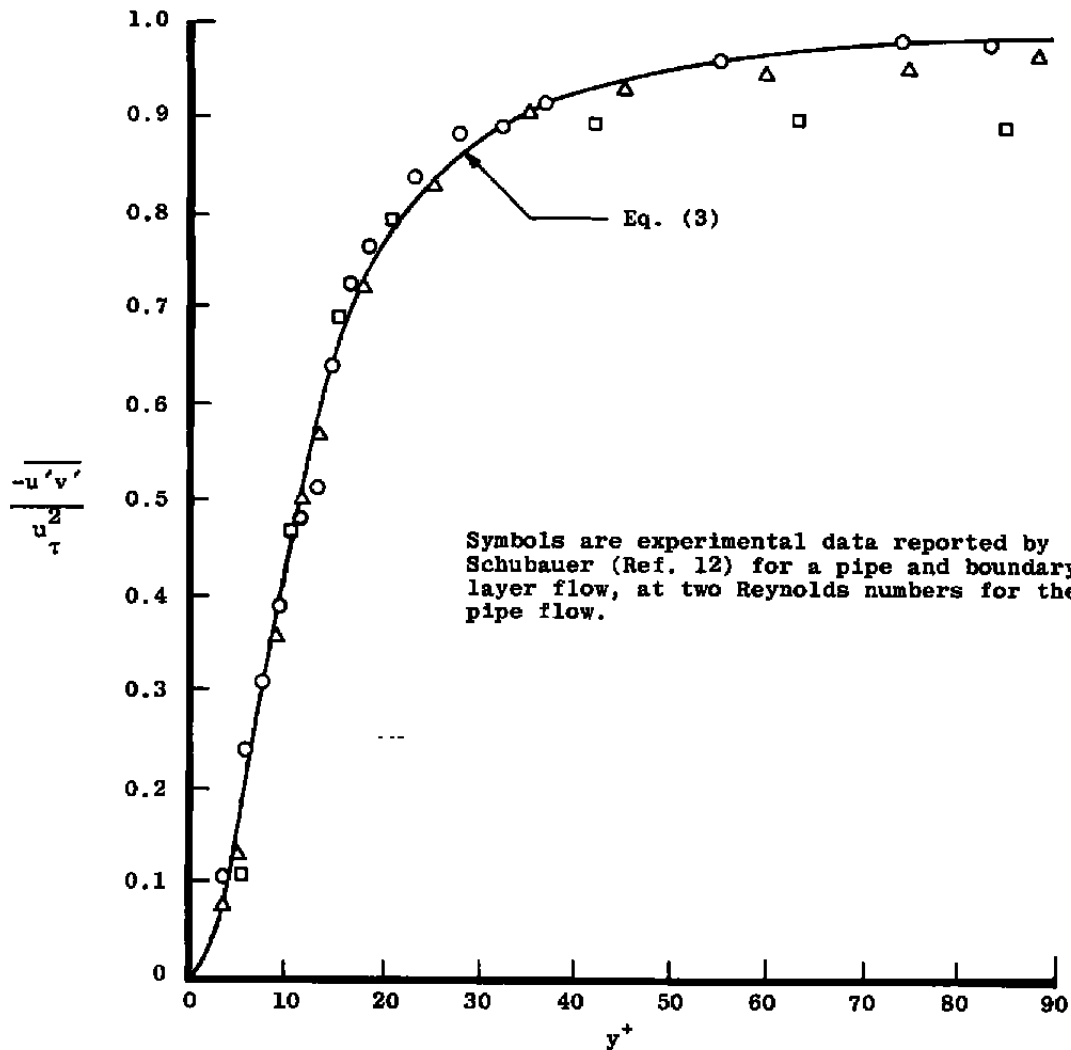


Figure 2. Reynolds stress distributions according to Eq. (3) and the experimental data reported by Schubauer (Ref. 12).

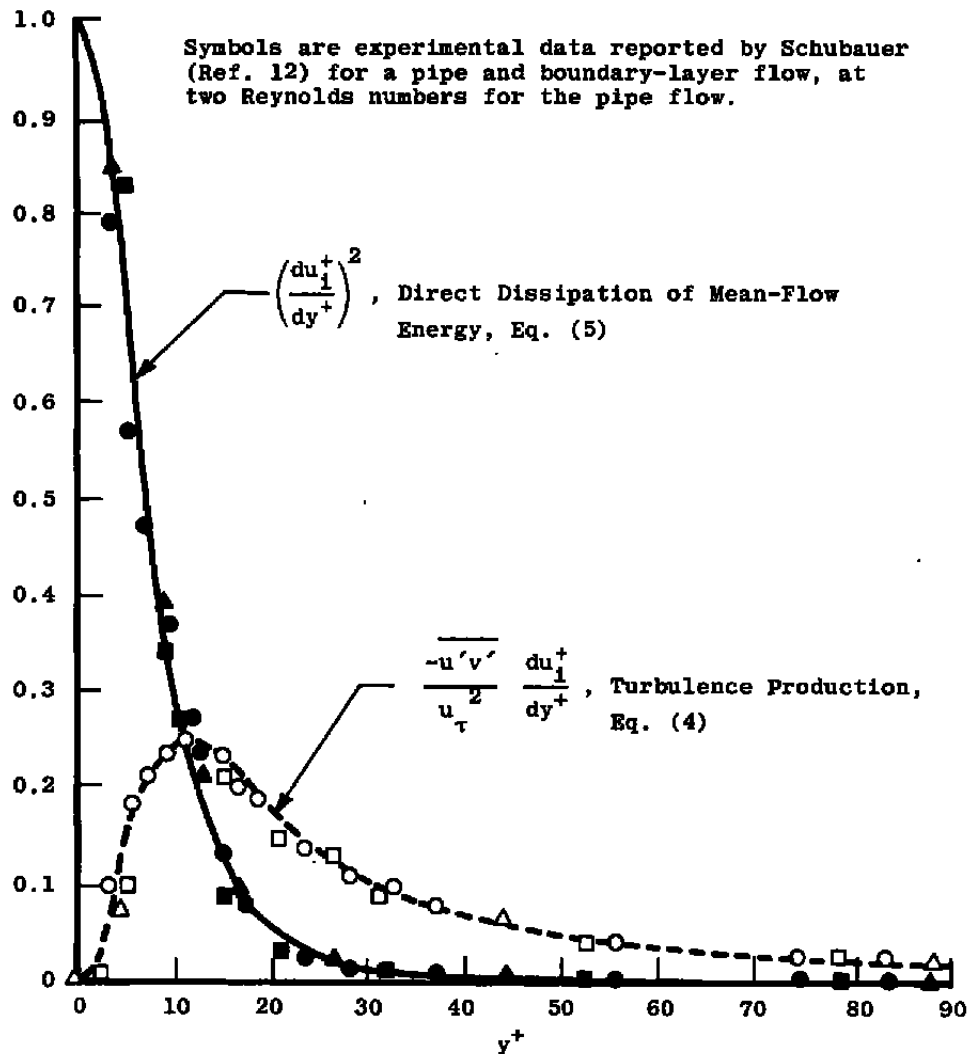


Figure 3. Turbulence production and dissipation distributions according to Eqs. (4) and (5) and the experimental data reported by Schubauer (Ref. 12).

<u>Sym</u>	<u><math>c_f \times 10^3</math></u>	<u>H</u>	<u><math>Re_\theta \times 10^{-3}</math></u>	<u>Source</u>
○	0.31	2.566	12.19	Stratford's Data (Ref. 6) Used in Eq. (6)
△	2.95	1.336	7.65	Bauer's Data (Ref. 6) Used in Eq. (6)
—	(c <sub>f</sub> , H, and Re <sub>θ</sub> are the same as each experiment)			Eq. (7), with a and b calculated as detailed in Table 1

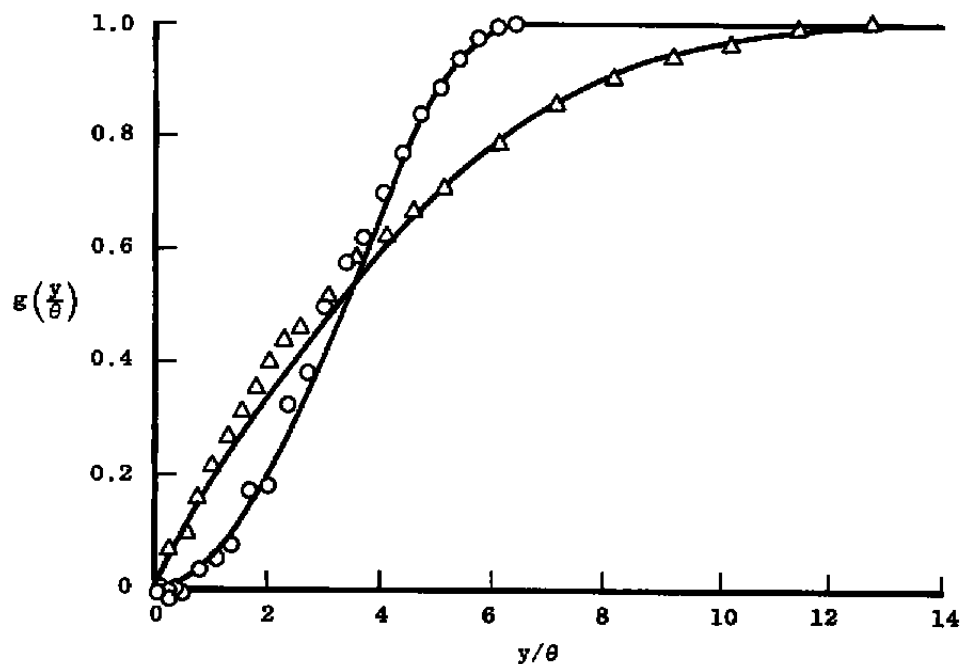
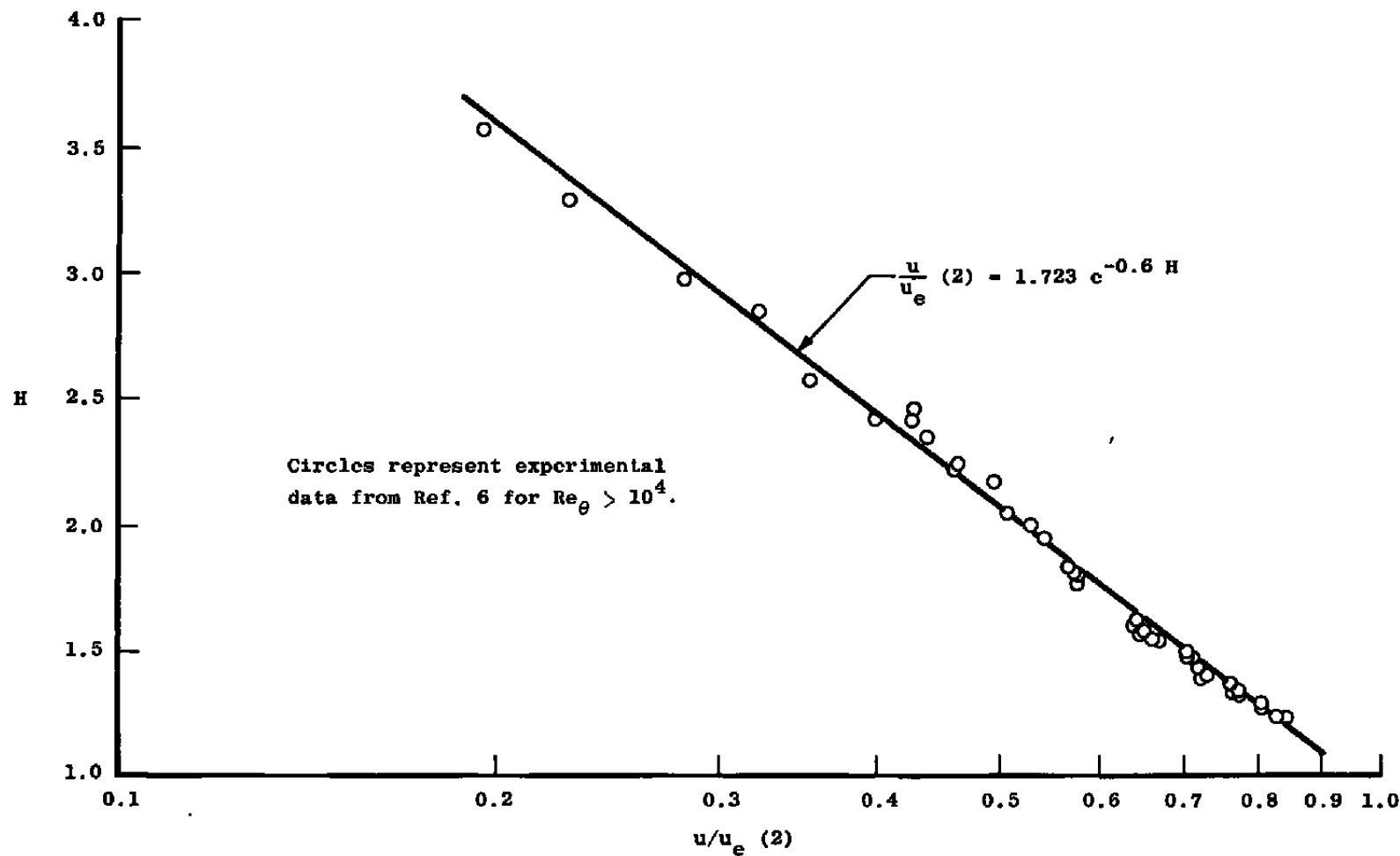
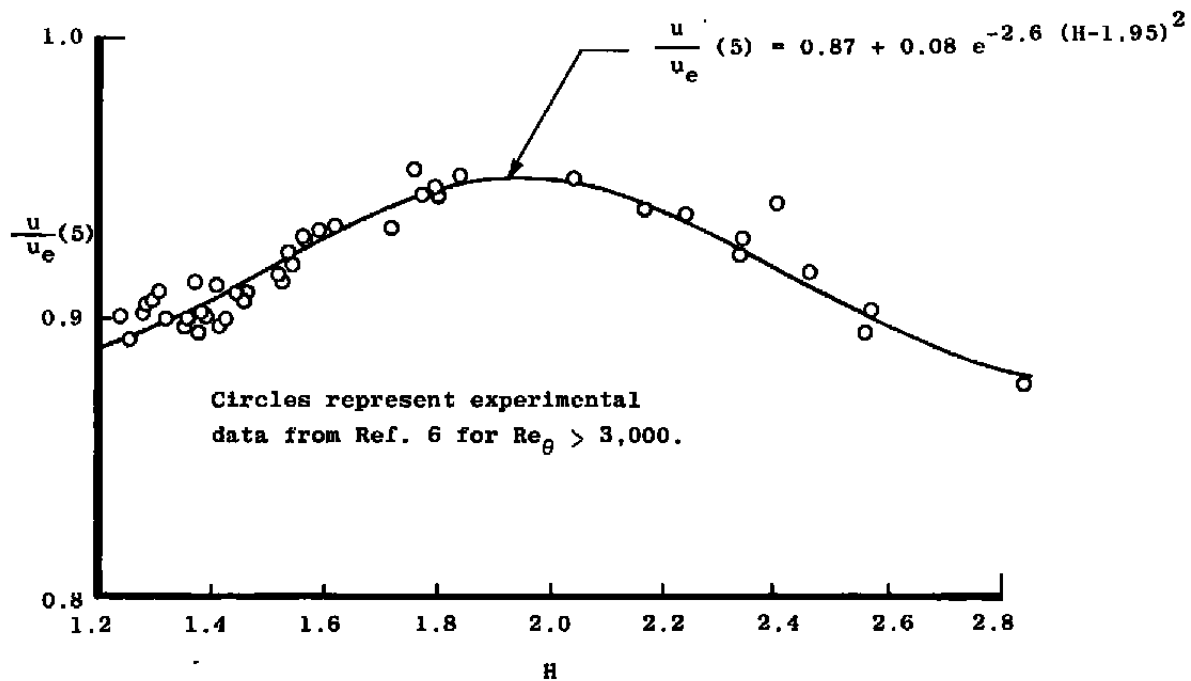


Figure 4. Distributions of the function  $g(y/\theta)$  according to Eqs. (6) and (7).



a.  $\gamma/\theta = 2$

Figure 5. Correlation of experimental velocity data.



b.  $y/\theta = 5$   
 Figure 5. Concluded.

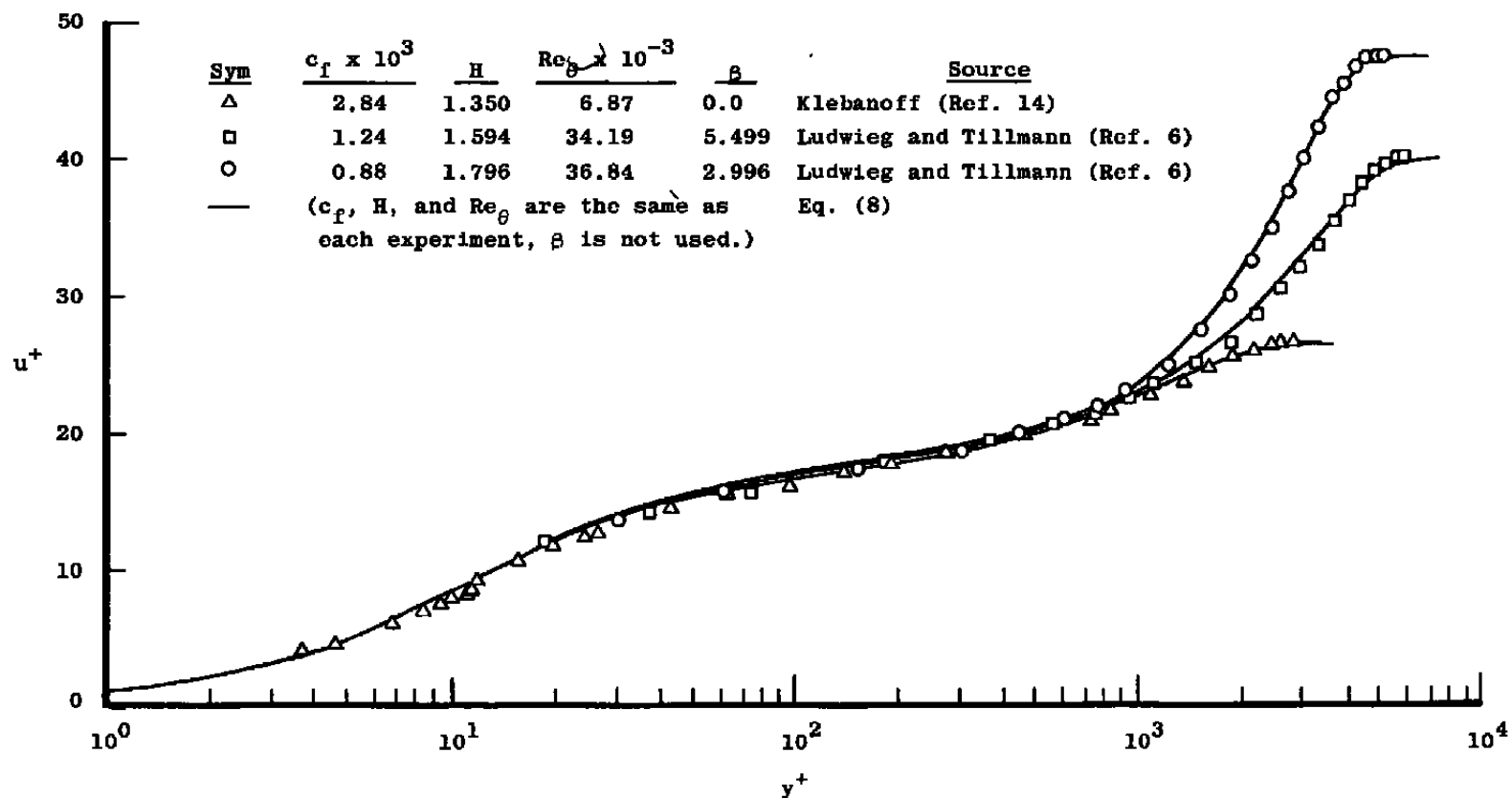


Figure 6. Zero, mild, and strong adverse pressure gradient boundary layers according to Eq. (8) and the experimental data of Klebanoff (Ref. 14) and Ludwig and Tillman (Ref. 6).



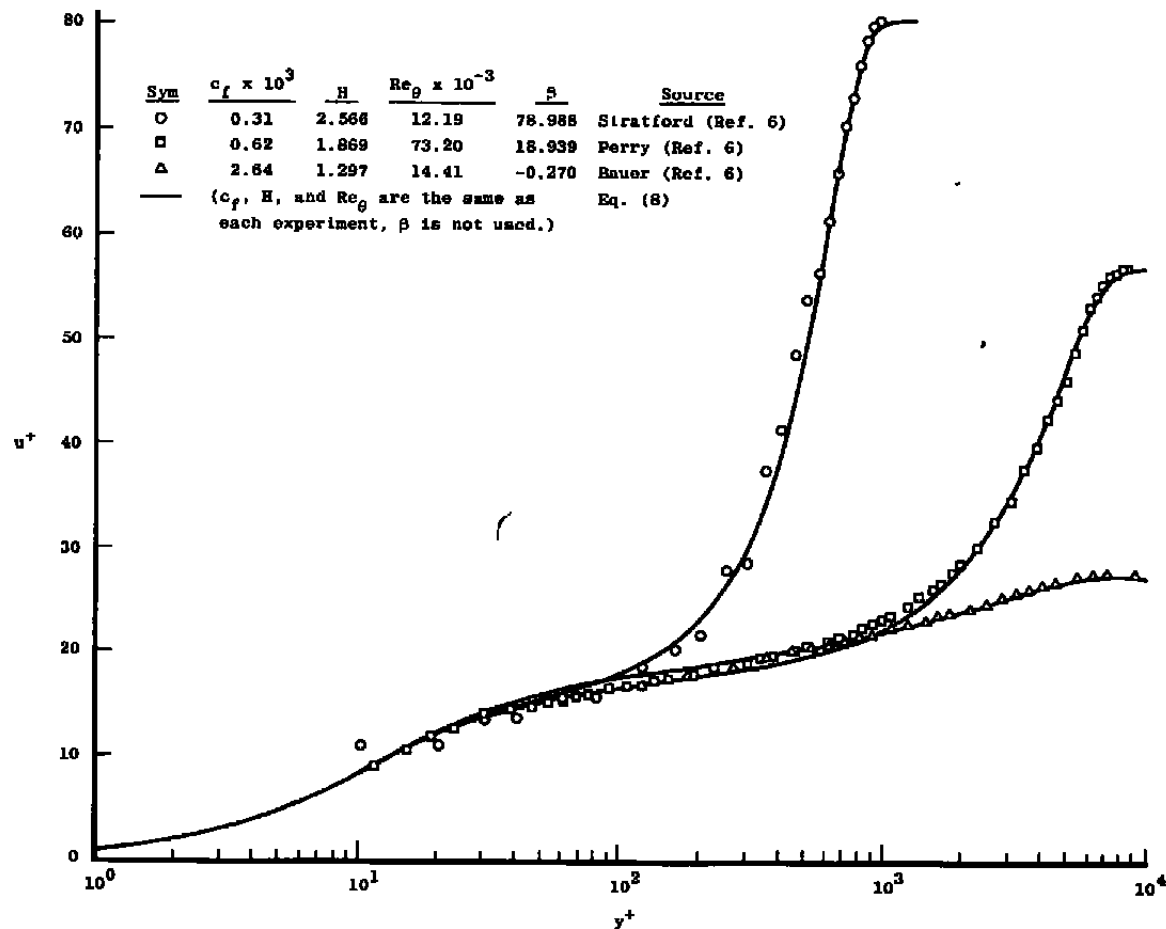


Figure 7. Adverse and favorable pressure gradient boundary layers according to Eq. (8) and the experimental data of Stratford (Ref. 6), Perry (Ref. 6), and Bauer (Ref. 6).

Sym	$c_f \times 10^3$	$H$	$Re_\theta \times 10^{-3}$	$\theta$	Source
○	2.94	1.386	4.44	0	Tillmann (Ref. 6)
□	0.28	2.546	9.29	44.577	Tillmann (Ref. 6)
◇	0.84	1.994	9.92	10.686	Tillmann (Ref. 6)
△	1.94	1.515	9.98	1.497	Tillmann (Ref. 6)

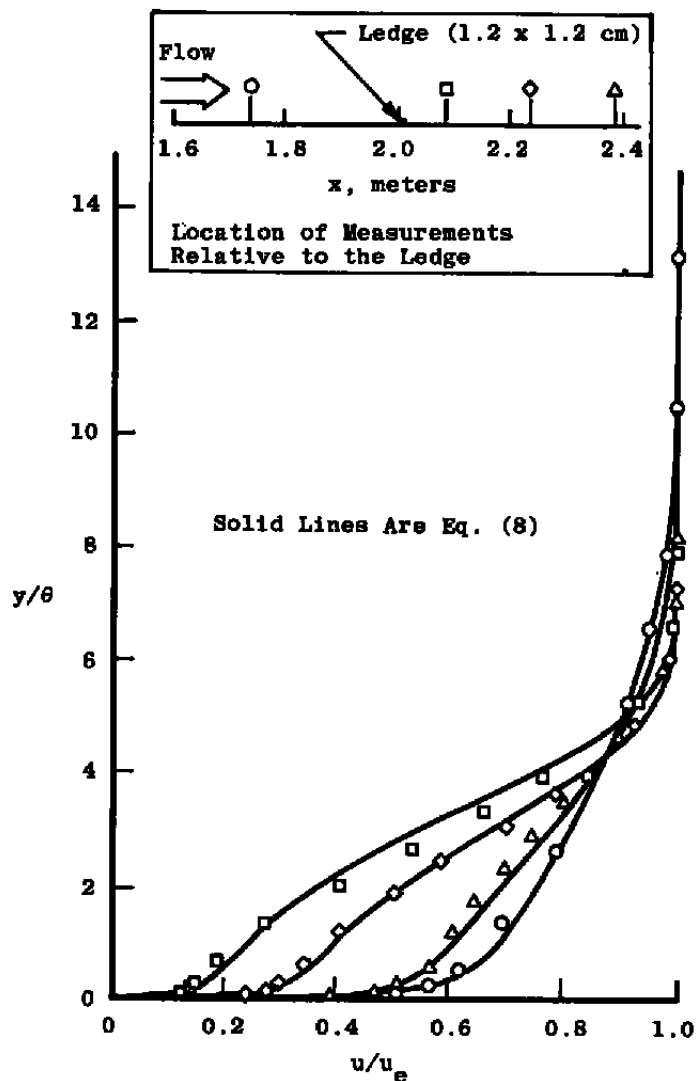


Figure 8. Comparisons of the experimental data of Tillman (Ref. 6) with Eq. (8) for boundary layers upstream and downstream of separation.

Sym	$c_f \times 10^3$	$H$	$Re_\theta \times 10^{-3}$	$\beta$	Source
O	0.91	1.837	17.37	14.541	Newman (Ref. 6)
□	0.18	2.455	26.33	182.776	Newman (Ref. 6)
—	(c <sub>f</sub> , H, and Re <sub>θ</sub> are the same as each experiment, β is not used.)				Eq. (8)

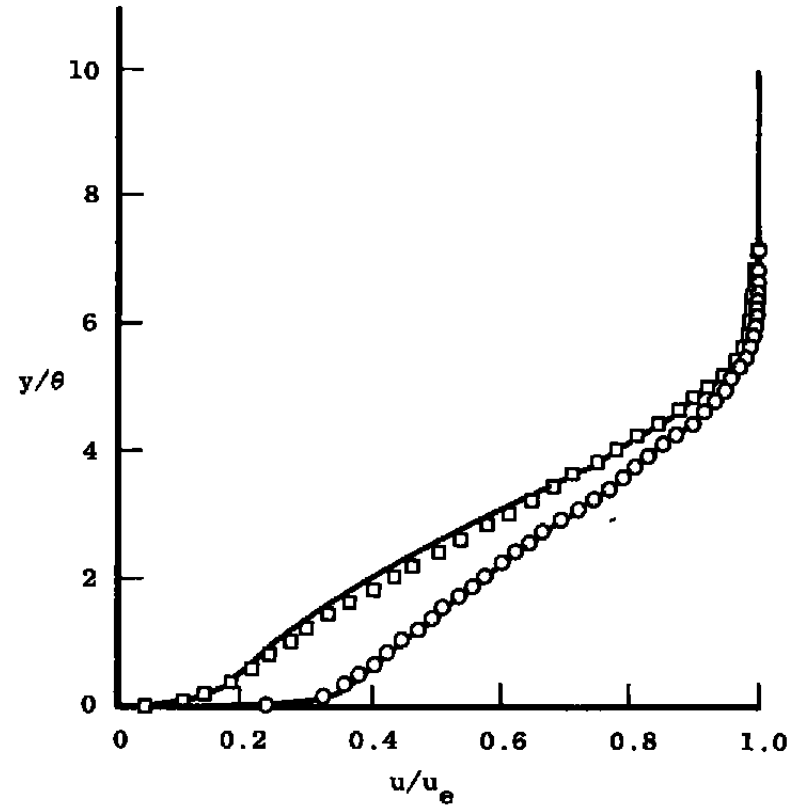


Figure 9. Airfoil boundary-layer flow proceeding toward separation in  $u/u_e$ - $y/\theta$  coordinates.

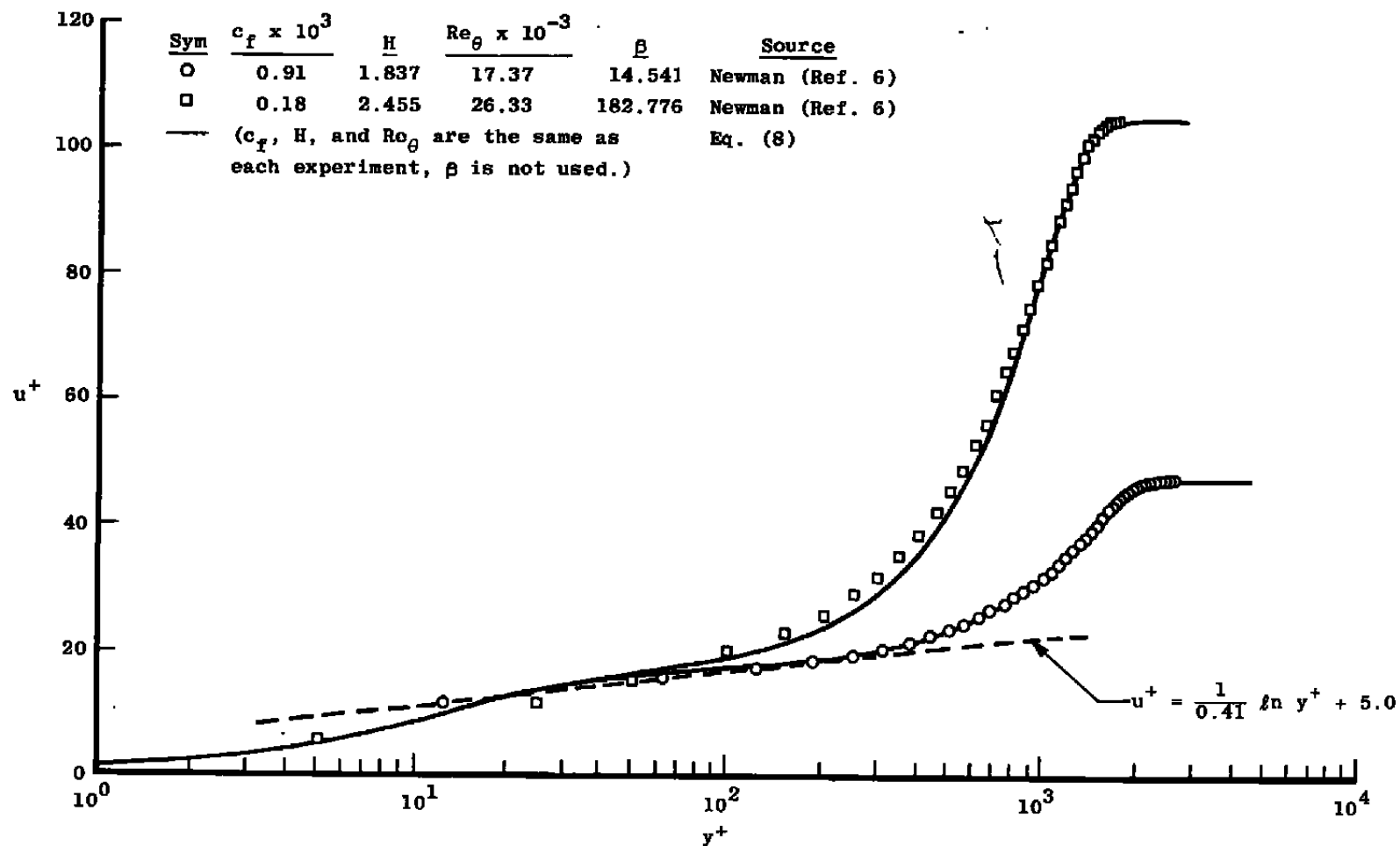


Figure 10. Airfoil boundary-layer flow proceeding toward separation in  $u^+$ - $y^+$  coordinates.

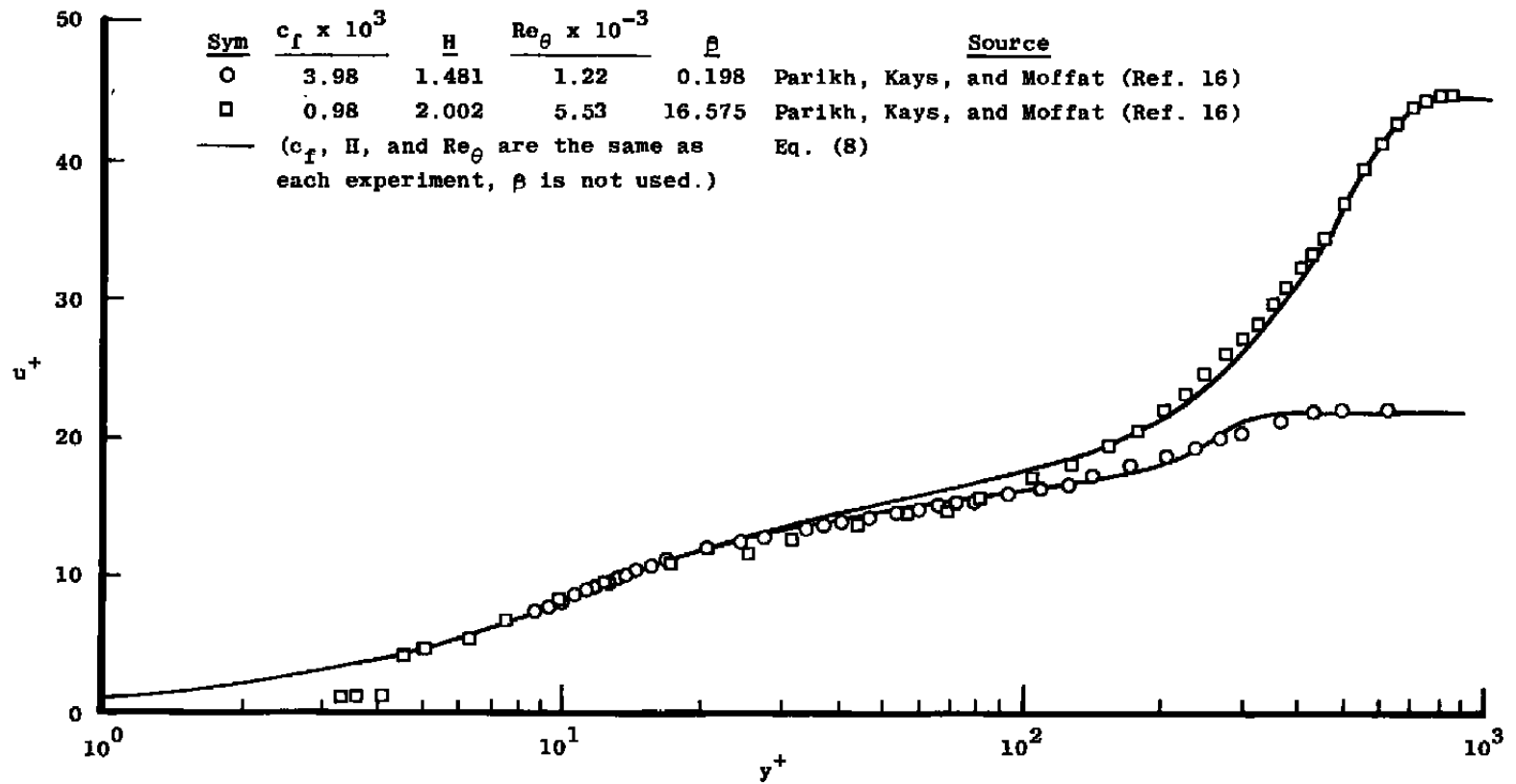


Figure 11. Low Reynolds number, nonequilibrium, adverse pressure gradient turbulent boundary layers according to Eq. (8) and the experimental data of Parikh, Kays, and Moffat (Ref. 16).

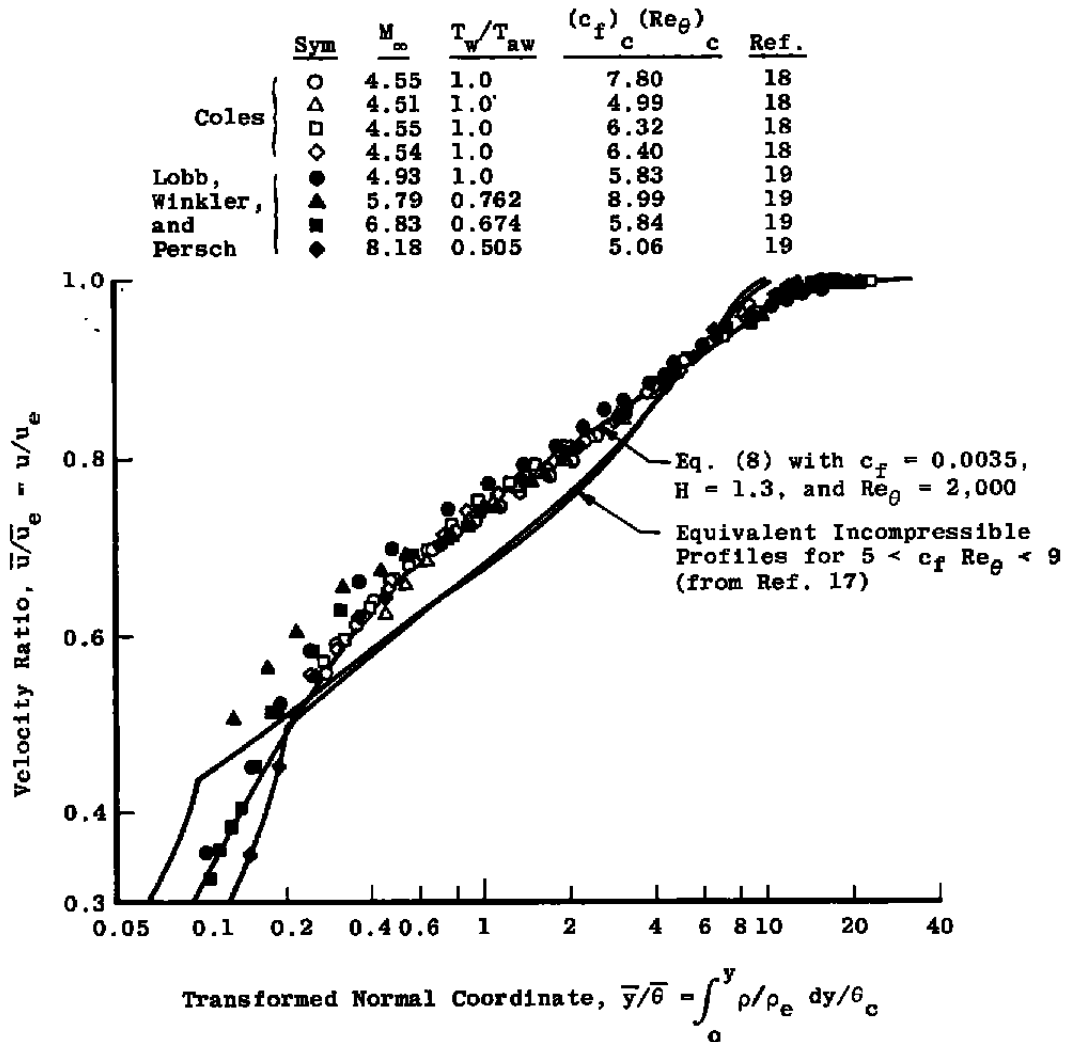


Figure 12. Experimental compressible turbulent boundary-layer data in transformed coordinates compared to Eq. (8).

Sym	$c_f \times 10^3$	$H_c$	$H$	$Re_\theta \times 10^{-3}$	$M_e$	Source
○	3.03	1.369	1.369	4.96	0.20	ART Data
□	2.29	1.580	1.360	22.96	0.65	ART Data
— ( $c_f$ , $H$ , and $Re_\theta$ are the same in each experiment.)						Eq. (8)

Measurement by  
Dr. J. A. Benek,  
ARO, Inc.

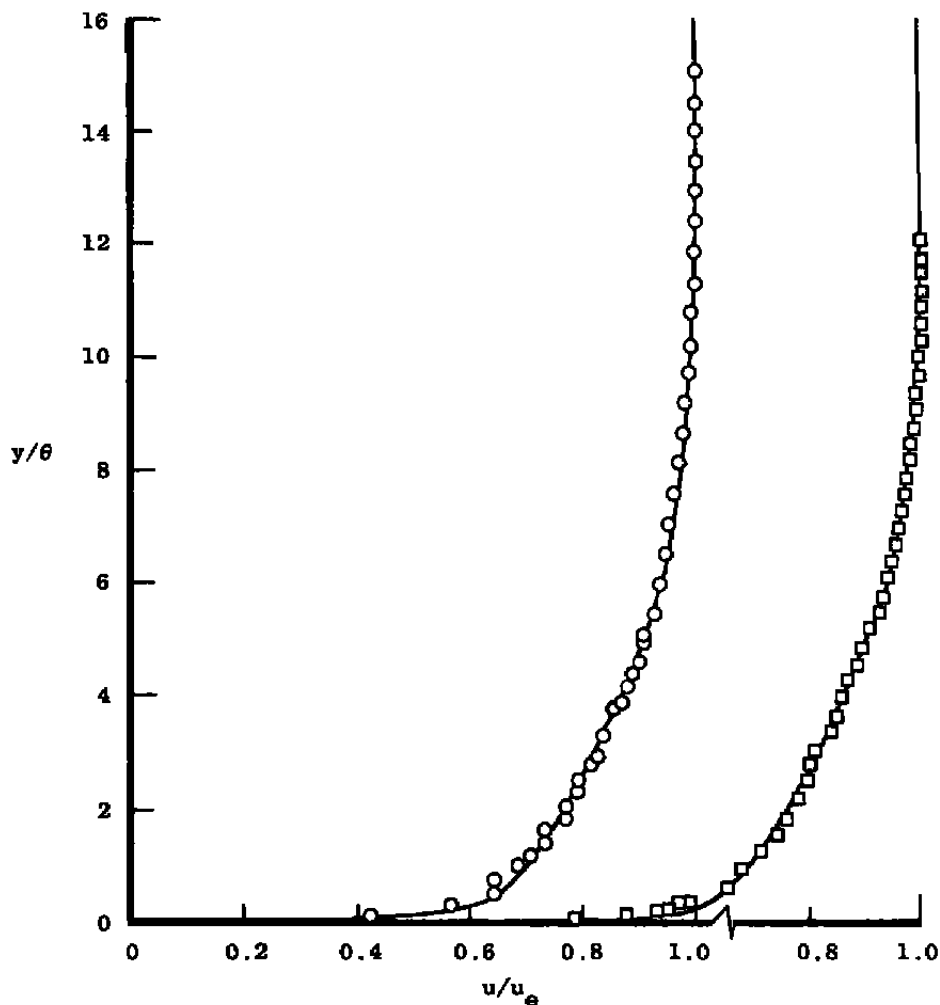


Figure 13. Acoustic Research Tunnel (ART) wall boundary-layer measurements at Mach numbers of 0.20 and 0.65 compared to Eq. (8).

Sym	$c_f \times 10^3$	$H_c$	H	$Re_\theta \times 10^{-3}$	$M_e$	Source
○	2.10	1.550	1.303	26.47	0.73	Altstatt (Ref. 22)
□	1.37	1.673	1.502	40.96	0.61	Altstatt (Ref. 22)
— ( $c_f$ , H, and $Re_\theta$ are the same as each experiment.)						Eq. (8)

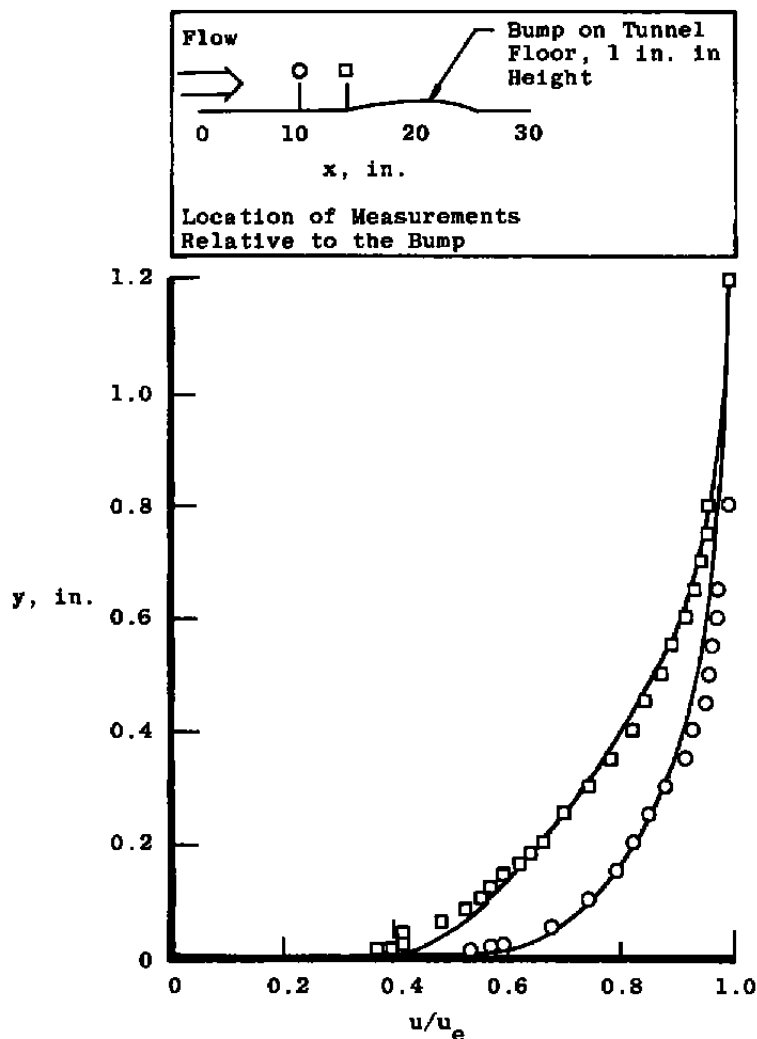


Figure 14. LV data from the Aerodynamic Wind Tunnel (1T) (Tunnel 1T) bump experiments (Ref. 22) compared to Eq. (8).



**Table 1. Summary of Procedure for Computation of Turbulent Boundary-Layer Velocity Distributions**

Step	Requirement	Comment
1.	$H$ , $u_e^+$ , and $Re_\theta$ are inputs (use incompressible values)	$u_e^+ = \left(\frac{2}{c_f}\right)^{\frac{1}{2}}$
2.	Compute $\frac{u}{u_e}(2) = 1.723 e^{-0.6 H} \left(1 + \frac{50}{Re_\theta}\right)$	$\frac{u}{u_e} \left(\frac{y}{\theta}\right)$ at $\frac{y}{\theta} = 2$
3.	Compute $\frac{u}{u_e}(5) = 0.87 + 0.08e^{-2.6(H-1.95)^2}$	$\frac{u}{u_e} \left(\frac{y}{\theta}\right)$ at $\frac{y}{\theta} = 5$
4.	Compute $g(2) = \frac{\frac{u}{u_e}(2) - \frac{1}{0.09 u_e^+} \tan^{-1} \left(\frac{0.18 Re_\theta}{u_e^+}\right)}{1 - \frac{\pi}{0.18 u_e^+}}$	$g\left(\frac{y}{\theta}\right)$ at $\frac{y}{\theta} = 2$
5.	Compute $g(5) = \frac{\frac{u}{u_e}(5) - \frac{1}{0.09 u_e^+} \tan^{-1} \left(\frac{0.45 Re_\theta}{u_e^+}\right)}{1 - \frac{\pi}{0.18 u_e^+}}$	$g\left(\frac{y}{\theta}\right)$ at $\frac{y}{\theta} = 5$
6.	Compute $b = \frac{\ln \left( \frac{\tanh^{-1} [g^2(2)]}{\tanh^{-1} [g^2(5)]} \right)}{\ln \left( \frac{2}{5} \right)}$	$\tanh^{-1} z = \frac{1}{2} \ln \left( \frac{1+z}{1-z} \right)$ $\tanh z = \frac{e^{2z} - 1}{e^{2z} + 1}$
7.	Compute $a = \frac{\tanh^{-1} [g^2(2)]}{2^b}$	
8.	$u^+ = \frac{1}{0.09} \tan^{-1} (0.09 y^+) + (u_e^+ - \frac{\pi}{0.18}) \tanh^{\frac{1}{2}} \left[ a \left(\frac{y}{\theta}\right)^b \right]$	$\frac{u}{u_e} = \frac{u^+}{u_e^+}$ and $y^+ = \frac{Re_\theta}{u_e^+} \frac{y}{\theta}$

## NOMENCLATURE

$a$	Parameter in Eqs. (7) and (8)
$b$	Parameter in Eqs. (7) and (8)
$c_f$	Local skin friction coefficient, $2\tau_w/\rho_e u_e^2$
$g$	Function defined by Eq. (7)
$H$	$\delta^*/\theta$
$M$	Mach number
$p$	Static pressure
$Re_\theta$	$\rho_e u_e \theta / \mu_e$
$u$	Mean velocity in the x direction
$u_\tau$	$(\tau_w/\rho_w)^{1/2}$
$u^+$	$u/u_\tau$
$u_1^+$	Inner solution for $u^+$
$u_o^+$	Outer expression for $u^+$
$\bar{u}/u_e$	Defined by Eq. (11)
$-\overline{u'v'}$	Reynolds stress
$x$	Coordinate along body surface

$y$	Coordinate normal to body surface
$y^+$	$u_{\tau w} \rho y / \mu_w$
$\overline{y}/\theta$	Defined by Eq. (12)
$\beta$	$\frac{\delta^*}{\tau_w} \frac{dp}{dx}$
$\delta$	Boundary-layer thickness
$\delta^*$	Boundary-layer displacement thickness
$\theta$	Boundary-layer momentum thickness
$\mu$	Molecular viscosity
$\Pi$	Coles' profile parameter
$\rho$	Density
$\tau$	Total shear stress

## SUBSCRIPTS

$c$	Compressible value
$e$	Boundary-layer edge value
$w$	Wall value
$aw$	Adiabatic wall value